Article

Effective Removal of Pb(II) from Multiple Cationic Heavy Metals—An Inexpensive Lignin-Modified Attapulgite

Shuai Guo [1,2,3], Wei Zhang [4,*], Yunguo Liu [4], Shiyong Tan [2,3], Hao Cai [2,3], Jing Geng [4] and Xuanming Liu [1,*]

[1] Hunan Province Key Laboratory of Plant Functional Genomics and Developmental Regulation, College of Biology, Hunan University, Changsha 410012, China; colin42kwok@gmail.com
[2] Hunan Engineering Research Center of Safe and Efficient Utilization of Heavy Metal Contaminated Arable Land, Changsha 410083, China; shiy-tan@hotmail.com (S.T.); hawkcaihao@gmail.com (H.C.)
[3] Biological Fertilizer Engineering Technology Research Center of Hunan, Changsha 410205, China
[4] College of Environmetal Science & Engineering, Hunan University, Changsha 410012, China; liuyunguo@hnu.edu.cn (Y.L.); jinggeng2023@163.com (J.G.)
* Correspondence: zhangweisx@hnu.edu.cn (W.Z.); xml05@hnu.edu.cn (X.L.)

Abstract: To develop cost-effective heavy metal adsorbents, we employed water-soluble lignin from black liquor to modify activated attapulgite, resulting in the creation of a novel adsorbent called Lignin-modified attapulgite (LATP). In this study, scanning electron microscopy and Fourier transform infrared spectrometer techniques were utilized to characterize the structural details of LATP. The results revealed that lignin occupies the micropores of attapulgite, while additional functional groups are present on the attapulgite surface. We conducted adsorption tests using LATP to remove five types of heavy metal ions (Cd^{2+}, Pb^{2+}, Zn^{2+}, Mn^{2+}, Cu^{2+}), and it was found that LATP exhibited greater removal mass and binding strength for Pb(II) compared to the other ions. For further investigation, batch experiments were performed to evaluate the adsorptive kinetics, isotherms, and thermodynamics of Pb^{2+} removal from aqueous solutions using LATP. The results indicated that the adsorption capacity of Pb(II) on LATP decreased with decreasing pH, while the presence of Na^+ had no effect on adsorption. The adsorption process reached equilibrium rapidly, and the Langmuir adsorption capacities increased with temperature, measuring 286.40 mg/g, 315.51 mg/g, and 349.70 mg/g at 298 K, 308 K, and 318 K, respectively. Thermodynamic analysis revealed positive values for ΔH_0 and ΔS_0, indicating an endothermic and spontaneous adsorption process. Furthermore, ΔG_0 exhibited negative values, confirming the spontaneous nature of the adsorption. Consequently, LATP demonstrates great potential as an effective adsorbent for the removal of Pb(II). Therefore, LATP shows great potential as an effective adsorbent for the removal of Pb(II) from natural water environments, contributing to the sustainable development of man and nature.

Keywords: lignin; attapulgite; Pb(II); adsorption; selective adsorption; isotherms; thermodynamic

1. Introduction

Metals and metalloids with a density greater than 4.0 g cm^{-3} are defined as heavy metals such as Cd^{2+} and Pb^{2+} [1]. Non-essential heavy metals and essential heavy metals above a certain concentration are toxic to living organisms [2]. Heavy metals are natural elements, but heavy metal pollution has both natural and anthropogenic sources. Along with the tremendous progress and industrial development of human society, heavy metal pollution has become a global environmental issue. Scientists all over the world are looking for ways to solve heavy metal pollution and reduce their risk of pollution in order to protect the environment and human health, including various physical, chemical or biological techniques [3]. However, these methods are not completely able to solve the heavy metal pollution problem, most of which are still in the laboratory research stage, and the technology that is really used for large-scale engineering applications is lacking.

Therefore, there is an urgent need to research and develop a green, efficient, low-cost, and general-purpose scavenger for the removal of heavy metal contamination.

Heavy metal-contained wastewater is one of the most important and widespread sources of heavy metal pollution in soil. Many methods have been used to remove heavy metal ions from wastewater, such as chemical precipitation, adsorption, membrane filtration, coagulation and flocculation, flotation, and electrochemical treatment [4]. However, most of the methods are uneconomical and produce large quantities of chemical by-products that cause secondary pollution [5]. Adsorption is a cost-effective method for the removal of heavy metals from wastewater, and in recent years it has been shown to be cost-effective, green and applied at scale for production [6,7]. In contrast to advanced materials like graphene [8–10], biochar, and metal-organic frameworks (MOFs), nanoclays distinguish themselves with their natural sourcing, cost-effectiveness, environmental sustainability, and the ability to be tailored for specific pollutant adsorption through organic functionalization. They also exhibit robust thermal and chemical stabilities, allowing for their application in rigorous industrial environments. When it comes to evaluating costs, environmental considerations, or the need for chemical specificity, nanoclays often emerge as a more economical and pragmatic alternative. For the focus of this research, we have chosen attapulgite, a clay material that is not only cost-efficient but also renowned for its porous structure and expansive surface area, which lends itself well to adsorption applications. Attapulgite is a low-cost clay material with a porous structure and a large specific surface area that is commonly used for adsorption. The adsorption mechanism of attapulgite is dominated by physical adsorption, but physical adsorption is often not as stable as chemical adsorption. Chemisorption is usually much more efficient than physisorption [11,12], and the materials can be more effective in desorption and regeneration [13]. Therefore, Deng et al. and Qin et al. realized a chemisorption-dominated adsorption process for organically modified attapulgite [11,14]. Their organically modified attapulgite has excellent adsorption properties, but its source material cost and production cost are difficult to control.

The wide distribution, low toxicity, chemical stability and biodegradability of the biological matrices have gotten more research attention as carrier materials in recent years [15]. Lignin is a natural organic material commonly found in waste products from the paper industry. According to statistics, 130 million tons of kraft pulp and approximately 70 million tons of lignin are produced worldwide [16]. Only 5% of the available lignin has been exploited [17], indicating that there is enough low-cost lignin available for mining and utilization. Lignin is widely studied as a biosorbent for heavy metal ions [18,19]. The surface of lignin contains many functional groups, such as carboxylic and phenolic acids, which adsorb heavy metal ions by deprotonation [20], and it has a large adsorption capacity for heavy metal. However, it is difficult and expensive to separate lignin from black liquor by the conventional method [21]. In order to simplify the separation process of lignin and use it in wastewater treatment, this study isolated black liquor lignin by adsorbing acid-modified attapulgite.

In this study, a certain concentration of sulfuric acid was used to activate the natural attapulgite to obtain a larger pore size and specific surface area, which helped the attapulgite to have the ability to adsorb and fix lignin. Novel acid-modified lignin–attapulgite adsorbents can be simply prepared by adding acid-activated attapulgite to a lignin solution. The physical, chemical and structural properties of the adsorbents were characterized using characterization techniques such as scanning electron microscopy (SEM), Fourier transform infrared spectroscopy (FTIR), X-ray diffractometer (XRD), and thermogravimetric analysis (TGA). Systematic in-batch experiments were conducted to evaluate the effects of various influencing factors on the adsorption performance of the adsorbent.

2. Methods

2.1. Preparation of Lignin-Modified Attapulgite

Rice straw was crushed by using a high-speed crusher and through 20-mesh sieve and the straw powder was added to the boiling NaOH solution with the concentration of 4%, boiled for 10 min and then filtered through 5 layers of gauze and the filtrate (simulated black liquor) was taken and stored.

Attapulgite was added to H_2SO_4 solution (room temperature), and it should be stirred immediately to make the reactants evenly mixed and accelerate the release of gas. It was filtered with filter paper when there were no bubbles on the surface of the solution, and the filter residue (Activated attapulgite, AATP) was cleaned with deionized water for several times until neutral, grinded after drying and through 60 mesh sieve for later use.

The activated attapulgite was added to the lignin solution as the adding amount of 10%. When the surface of the solution was free of air bubbles, it was filtered with a vacuum extractor, and the filter residue (Lignin-modified attapulgite, LATP) was washed with deionized water for several times until neutral, and then it was dried at 60 °C for 24 h in a vacuum drying oven and ground, and then passed through a 60-mesh sieve for spare use.

2.2. Characterization of the Attapulgite Materials

The microscopic surface morphology of AATP and LATP samples was observed by SEM (ZEISS MERLIN Compact, Jena, Germany) to characterize structural details of the before and after immobilization. The functional groups of AATP and LATP samples were determined by FTIR (Nicolet iS5, Thermo Fisher Scientific, USA) in the range of 400–4000 cm^{-1} to explore the effect of immobilization on functional groups of materials. The material was tested for thermal gravity analysis by NETZSCH TG 209F3 (NETZSCH-Gerätebau GmbH, Germany). Zeta potentials were tested using a from Malvern Panalytical, UK. Brunauer, Emmett, and Teller (BET) were tested using a ASAP 2420 from Micromeritics, USA.

2.3. Batch Adsorption Experiments

The most suitable ions for adsorption by LATP were identified by testing the adsorption capacity of LATP on five heavy metals (Cd^{2+}, Pb^{2+}, Zn^{2+}, Mn^{2+}, Cu^{2+}). The contaminant solution is prepared by $Cd(NO_3)_2$, $Pb(NO_3)_2$ $Zn(NO_3)_2$, $Mn(NO_3)_2$ and $Cu(NO_3)_2$. Batch experiments were carried out for the adsorption process of the selected ions under different competitive ion concentrations, solution pH, contact time, initial concentration and temperature conditions. The pH of solutions was adjusted by 0.1 M HNO_3 or NaOH in the above tests. In this study, 0.1 g attapulgite materials were added to 250 mL conical flask containing 50 mL solution and shaken at a constant speed (160 r/min) in desirable times.

The mixtures were separated by centrifugation at 4000 r/min for 10 min and the concentrations of ion in the supernatant were measured by inductively coupled plasma atomic emission spectroscopy (ICP) (Perkinelmer Optima 8300, perkinelmer, USA) after shaking. The experiments were repeated three times and averaged.

The adsorption capacities of ions on LATP at any time (q_t; mg/g) and equilibrium (q_e; mg/g) were calculated by the following equations:

$$q_t = \frac{(c_0 - c_t)V}{m} \tag{1}$$

$$q_e = \frac{(c_0 - c_e)V}{m} \tag{2}$$

where c_0, c_t, and c_e are the ion concentration (mg/L) at beginning, any time t, and equilibrium, respectively;

V is the used volume (L) of solution; and m is the mass (g) of the adsorbent.

3. Results and Discussions

3.1. Adsorbent Properties

#### 3.1.1. Exploration of Surface Morphology of Materials

Scanning electron microscope (SEM) images of AATP and LATP show the morphological changes of the samples before and after lignin immobilization (Figure 1). The microstructure of ATP and AATP is characterized by agglomerated aggregates. Obviously, LATP after lignin loading had a more dispersed structure and did not agglomerate as much as ATP and AATP. This suggests that LATP may have a larger specific surface area. In addition, an abundant fiber structure appeared on the surface of LATP, suggesting that lignin successfully modified the surface of LATP and made it better dispersed.
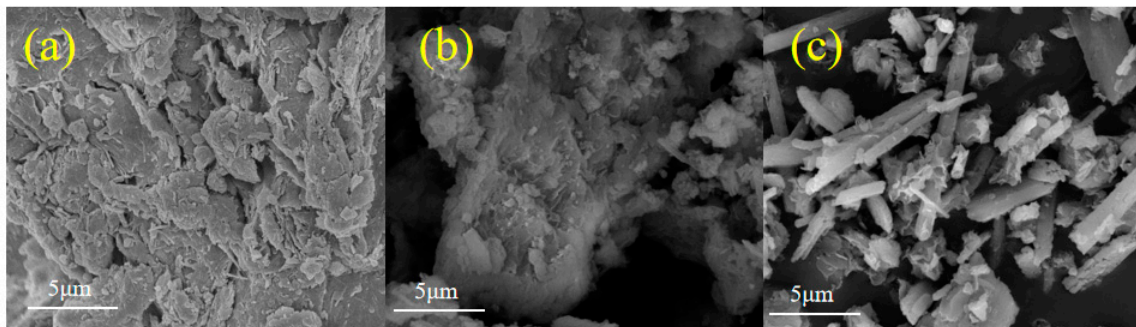
Figure 1. SEM images of ATP (**a**), AATP(**b**) and LATP (**c**) samples.

3.1.2. Characterization of Potential Reactive Groups on Material Surfaces

The FTIR spectrum of AATP and LATP is shown in Figure 2. The absorption bands at 3400–3610 cm^{-1} of the FTIR spectrum are assigned to the O-H stretching vibrations. The peaks in AATP at 3407, 3550, 3610 cm^{-1} were assigned to O-H stretching vibrations of structural water and other water molecules. The peaks in AATP became a wide band in LATP at 3436 cm^{-1} and the peak intensity increased significantly. The peak in LATP at 3436 cm^{-1} was assigned to hydroxy stretching in phenolic and aliphatic structures, which originated from lignin. It is similarly that the peaks in LATP at 1640 and 1466 cm^{-1} were assigned to aromatic conjugated C=O and benzene ring vibration, respectively, and the peak in LATP at 1032 cm^{-1} was assigned to the aromatic rings in the plane C-H bending. Moreover, there was a new peak in LATP at 1321 cm^{-1}, which was assigned to the aromatic ring breathing [22–25]. The above results indicate that lignin was immobilized on AATP and added a lot of functional groups to it, which is beneficial to its adsorption of heavy metal.
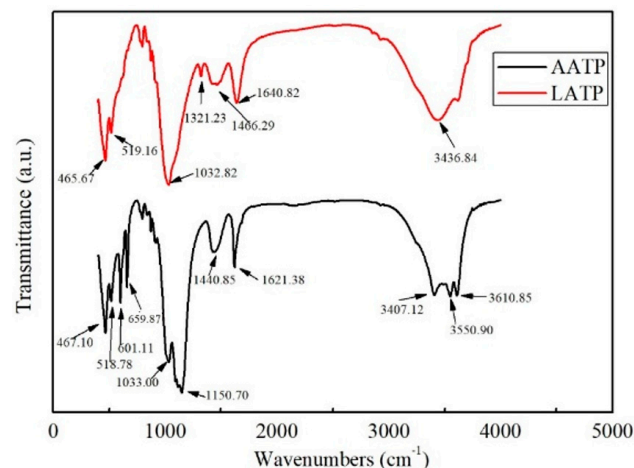
Figure 2. FTIR spectrum of AATP and LATP.

3.1.3. Pore Structure, Specific Surface Area and Elemental Analysis before and after ATP Modification

The Brunauer-Emmett-Teller (BET) parameter of ATP, AATP and LATP are listed in Table 1. LATP had the largest specific surface area, pore volume and average pore size of 168.872 cm^3/g, 0.220 cm^3/g and 8.138 nm, respectively. The results of the BET data indicate that H$_2$SO$_4$−mediated acid activation and lignin loading processes can both optimize the specific surface area and pore structure of ATP, increase the contact area of modified ATP with target pollutants, and potentially enhance the adsorption capacity of ATP.3.1.4 Zeta potential analysis for exploring the charge of materials. The increase in the porosity of LATP may be due to the release of volatile substances during the pyrolysis process, as well as the removal of soluble ash and soluble substances from the surface of attapulgite during the acidification process.

Table 1. Surface and structural characterizations of samples.

| Sample	Surface Area (m^2/g)	Pore Volume (cm^3/g)	Average Pore Radius (nm)
ATP	94.828	0.047	2.000
AATP	122.296	0.114	3.740
LATP	168.872	0.220	8.138

From the results of elemental analysis in Table 2, it can be seen that LATP has a higher content of elemental C/N/H compared to ATP, which indicates the successful loading of organic matter such as polycyclic aromatic hydrocarbons (PAHs) on lignin. The decrease in Al/Si/S/O content, on the other hand, may be attributed to the fact that some of the Si-Al structural layers of the concave lignite were eroded during the acidification process.

Table 2. XRF measurement of ATP and LATP.

Element	Conc.%	
	ATP	**LATP**
O	10.654	8.632
N	0.000	1.320
C	1.460	10.870
H	0.868	0.959
Si	50.677	46.190
Al	35.301	31.009
Others	1.04	1.02

3.1.4. Thermal Stability Analysis of Materials

The thermal weight-loss process of ATP is divided into four typical phases(Figure 3) [26]: (I) 0–200 °C, the first mass loss is very rapid and corresponds to the removal of bound water. (II) 200–300 °C, the second phase is also considered to be a slow removal phase of bound water, but this phase is reversible, which is attributed to the super-hydrophobicity of the clay. (III) 300–400 °C, with further increase in temperature, the water of crystallization between the aluminum-oxygen octahedra starts to be removed, and the structure of ATP starts to evolve into a rafter structure. (IV) When the temperature exceeds 500 °C, the fourth thermal weight loss is thought to be caused by the dehydroxylation of the Mg-OH structure of ATP, at which point the structure of ATP starts to collapse gradually [27]. It should also not be overlooked that the unstable carbonates in ATP may also lead to weight loss under thermal decomposition. ATP lost about 15.72% of its weight during the temperature increase from 0 to 800 °C.
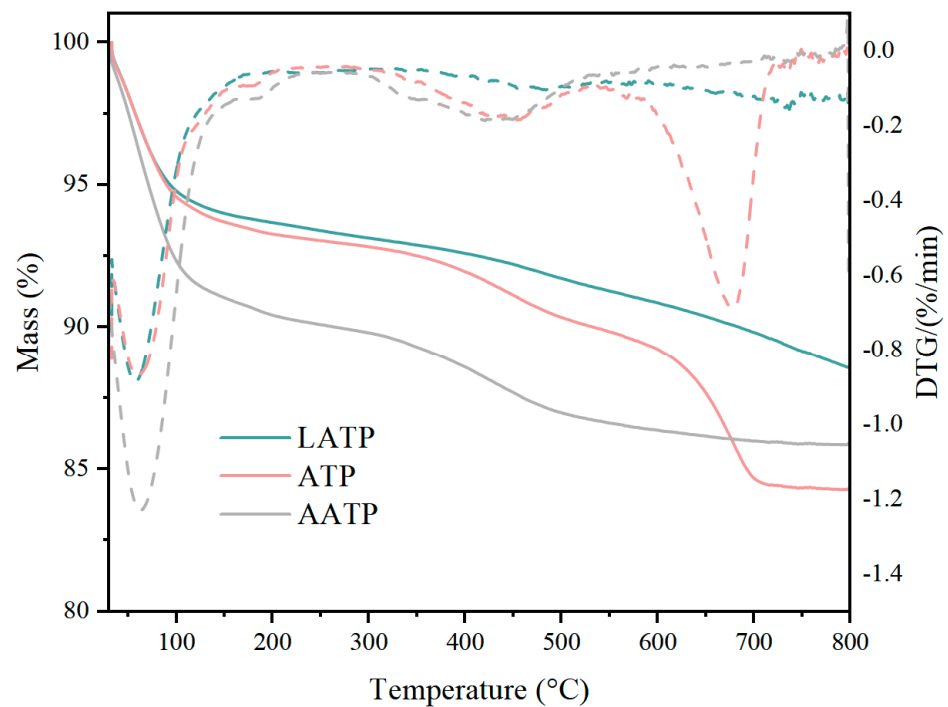
Figure 3. Thermogravimetric curves of ATP, AATP and LATP. The solid line represents the weight change corresponding to the left *Y*-axis. The dashed line represents the rate of weight loss, corresponding to the right *Y*-axis.

LATP only lost about 11.43% of its weight during the same warming process as ATP. At 0–200 °C, LATP exhibited bound water removal consistent with ATP. And at 200–500 °C, LATP showed a more uniform weight loss. At temperatures above 500 °C, LATP also did not show the same high rate of weight loss as ATP; this may be due to the elimination of carbonates during acidification. This suggests that Lignin-modified ATP has better thermal stability.

3.2. Adsorption Performance

3.2.1. Adsorption of Heavy Metal Ions

The adsorption capacity of LATP to five kinds of heavy metal ions (Cd^{2+}, Pb^{2+}, Zn^{2+}, Mn^{2+}, Cu^{2+}), ATP and AATP for Pb^{2+} were tested separately. The accurately weighed 0.100 g LATP were added to solutions of heavy metal ions, respectively. In each experimental group that was set up, pH, ion concentration and solution volume were kept consistent. The mixtures were separated by centrifugation after shaking for 4 h, and the concentrations of ions in the supernatant were measured.

The adsorption capacity of LATP to five kinds of heavy metal ions is shown in Figure 4, Figure 4a,b show the adsorption capacities, which were calculated by mass and molar mass, respectively. Adsorption capacities calculated by mass were the removal mass of heavy metals, and adsorption capacities calculated by molar mass were the numbers of adsorbed ions, which reflect the binding strength of ions. As seen from Figure 4, the adsorption capacities calculated by mass decreased in order Pb(II) > Cd(II) > Cu(II) > Mn(II) > Zn(II), the adsorption capacities calculated by molar mass decreased in order Pb(II) > Cu(II) > Cd(II) > Mn(II) > Zn(II). From the above results, it can be seen that LATP has a certain removal ability for a variety of cationic heavy metal pollutants, among which the removal quality and binding strength of Pb(II) are the strongest, which suggests that LATP has selective adsorption ability for Pb(II). This could be due to the fact that the hydration radius (4.01 Å) and the negative logarithm of the hydrolysis constant (7.71) of Pb(II) are smaller than those of several other heavy metals. These specific properties of the metal may facilitate the adsorption of Pb(II) onto LATP more readily through both inner surface

complexation and adsorption reactions [28,29]. Therefore, we chose lead (II) as the target pollutant and further investigated its adsorption mechanism in the following and studied the effect of multiple reaction parameters on it. We then explored the adsorption capacity of ATP and AATP for Pb^{2+}. LATP exhibited significantly higher adsorption capacity for Pb^{2+} compared to ATP and AATP.
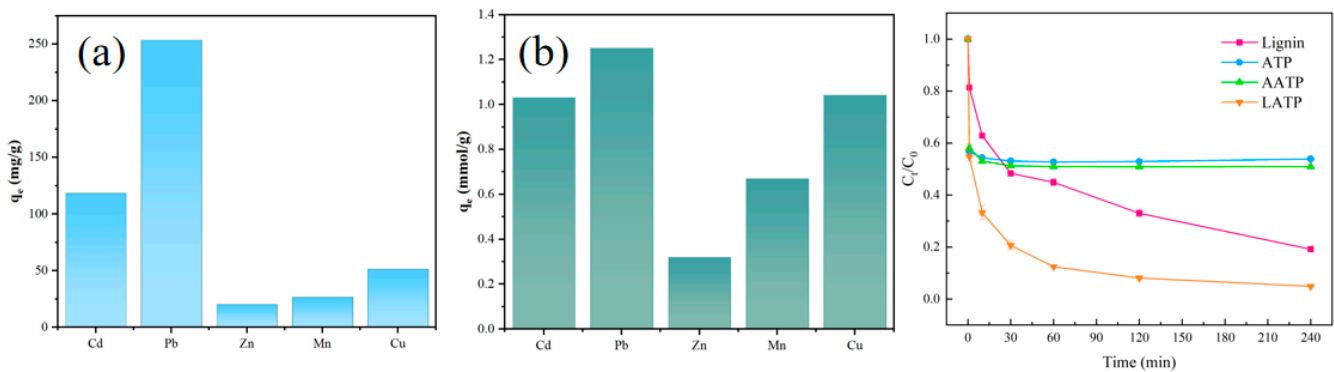
Figure 4. Adsorption capacities of different heavy metals on LATP, calculated by (**a**) mass and (**b**) molar mass,(**c**) adsorption capacity of different materials for Pb. (C_0 = 600 mg/L, T = 298 K, m = 2.0 g/L, V = 50 mL, pH = 4.5).

3.2.2. Competitive Adsorption Effects of Alkali Metal Ions

The removal efficiency of heavy metal ions is greatly influenced by competitive adsorption on the adsorbent surface, which is due to the presence of coexisting ions in solution [30]. Alkali metal ions such as Na^+ and K^+ are highly chemically active and are representative ions in competitive adsorption studies. It was reported that the Na^+ concentration increased from 0.001 mol/L to 0.1 mol/L making the adsorption rate of Pb(II) on palygorskite decrease by about 80% [31]. The effect of coexisting Na^+ on the adsorption of Pb(II) onto LATP was tested, and the results are shown in Figure 5. The results showed that no apparent effect was observed in the adsorption capacities of Pb(II) onto LATP when the concentrations of Na^+ increased from 0.005 mol/L to 0.025 mol/L.
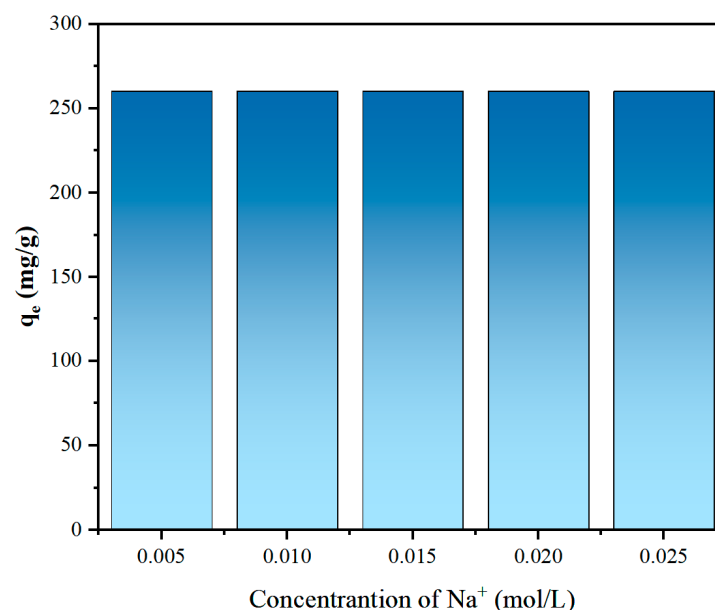
Figure 5. Effect of coexisting Na^+ on adsorption of Pb(II) onto LATP. (C_0 = 600 mg/L, T = 298 K, m = 2.0 g/L, V = 50 mL, pH = 4.5).

### 3.2.3. Effect of pH on the Adsorption Behavior of LATP

The surface charge properties of the adsorbent and the form of the adsorbate change with the solution pH, which can promote or inhibit the adsorption of heavy metals [32]. The pH of Pb(II) solutions was set at 1.0 to 7.0 to investigate the adsorption capacities of LATP for Pb(II) at different pHs, and the results were shown in Figure 6. The adsorption capacities increased with the increase in pH of solutions, which shows the low pH inhibited (pH = 1~2) absorption. It is due to the large amounts of H^+ and H_3O^+ in the solution will compete with the adsorption sites on the surface of the adsorbent, leading to protonation of the adsorbent surface, which will lose most of the adsorption capacity for Pb(II) [33]. Functional groups such as hydroxyl, carboxyl and amino groups in the adsorbent will be difficult to dissociate due to the large number of protons in the solution, thus failing to exert their adsorption capacity. In addition, the high concentration of protons in the solution will also bind to the groups on the surface of the adsorbent, thus presenting a positively charged surface of the adsorbent and making it difficult for Pb^{2+} to bind to the adsorbent [34]. Therefore, a slight decrease in adsorption capacity was observed when the pH was decreased from 7.0 to 3.0, indicating that LATP has a buffering capacity for acids and can be used in weak acid conditions. And when the pH value was further decreased, the adsorption capacity of LATP on Pb(II) decreased significantly, which may be due to the protonation on the surface of LATP under strong acid conditions.
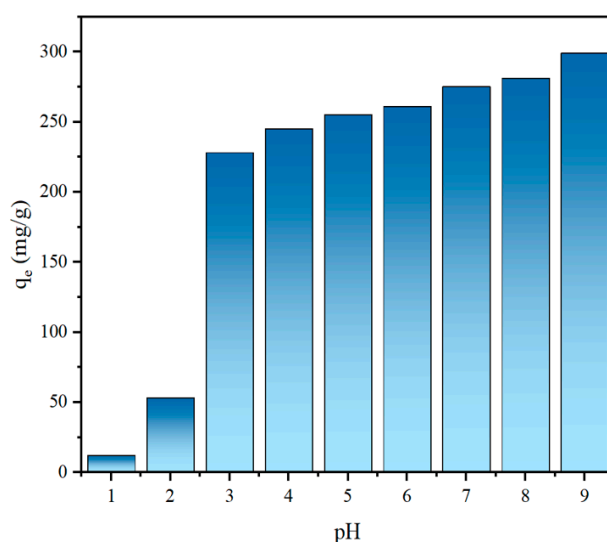
Figure 6. Effect of acidic conditions on the adsorption of Pb(II) by LATP. (c_0 = 700 mg/L, T = 298 K, m = 2.0 g/L, V = 50 mL).

The zeta potential can also be used to explain the effect of solution pH on adsorption (Figure 7). Lignin, ATP and LATP were all observed to have maximum zeta potential values at pH 5 (all negative). The reason for lignin exhibiting a negative zeta potential is mainly attributed to the free phenolic hydroxyl groups it carries [35]. The reason for the negative zeta potential of attapulgite may be due to its crystal structure, as the aluminum-oxygen octahedra in its structure are mainly surrounded by silica-oxygen tetrahedra, and excessive exposure of the silica-oxygen tetrahedra would cause the outer surface of attapulgite to be negatively charged, similar to the structure of halloysite [36]. The ATP-modified LATP possesses lower zeta potential than ATP, which is also probably due to the fact that lignans with abundant free phenolic hydroxyl groups resulted from the successful modification of lignin. As the pH increased to 9, a decrease in zeta potential values occurred to varying degrees for all three materials, with the lowest (−15.0 mV) for LATP. The results indicate that solution pH affects the charge value of the adsorbent surface, and as pH increases, the electronegativity of the adsorbent surface increases, possessing a stronger ability to remove Pb(II), which is consistent with the results demonstrated by the pH experiments.
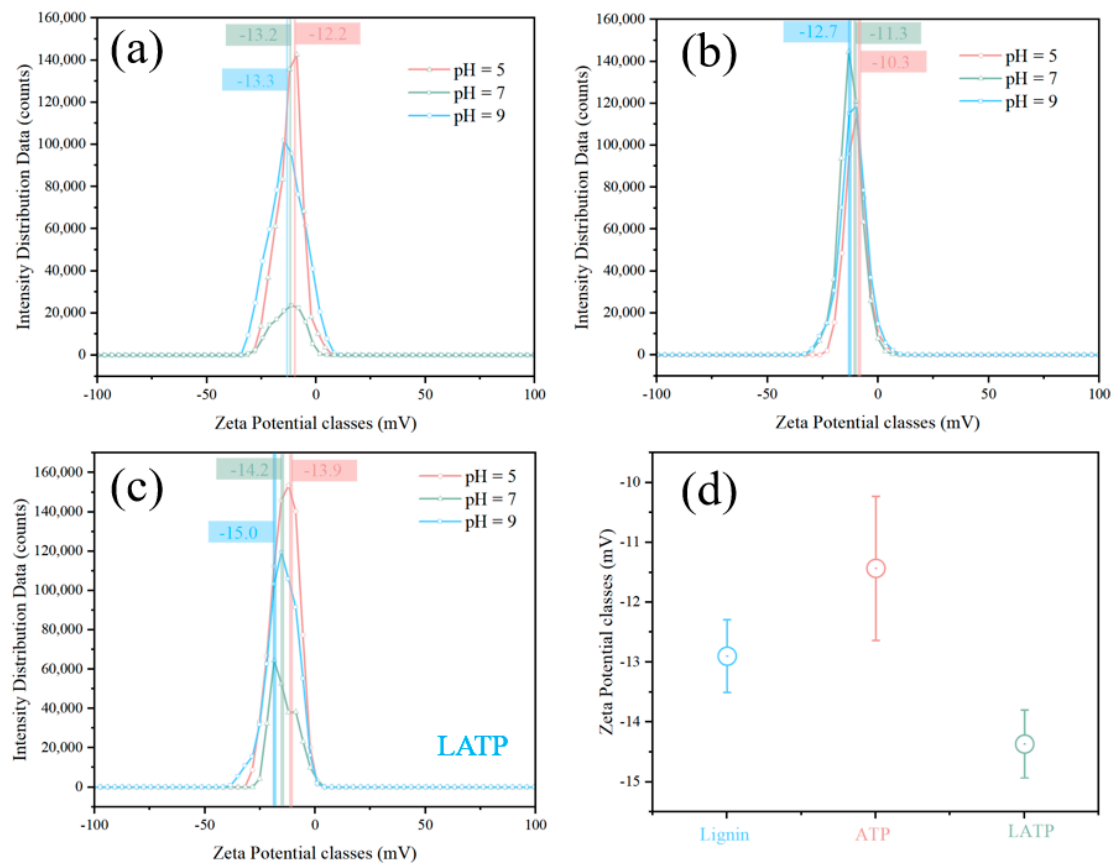
Figure 7. (**a**–**c**). Effect of initial solution pH on the zeta potential of the adsorbent. (**d**). Longitudinal comparison of zeta potential of each adsorbent.

3.2.4. Adsorption Kinetics of Pb(II)

The adsorption capacity of Pb(II) on LATP at different contact time were tested and the results are shown in Figure 8. The adsorption process occurred very rapidly at the initial contact time, Pb^{2+} in the solution were removed approximately 50% within 5 min and the adsorption equilibrium was reached at 120 min of contact.
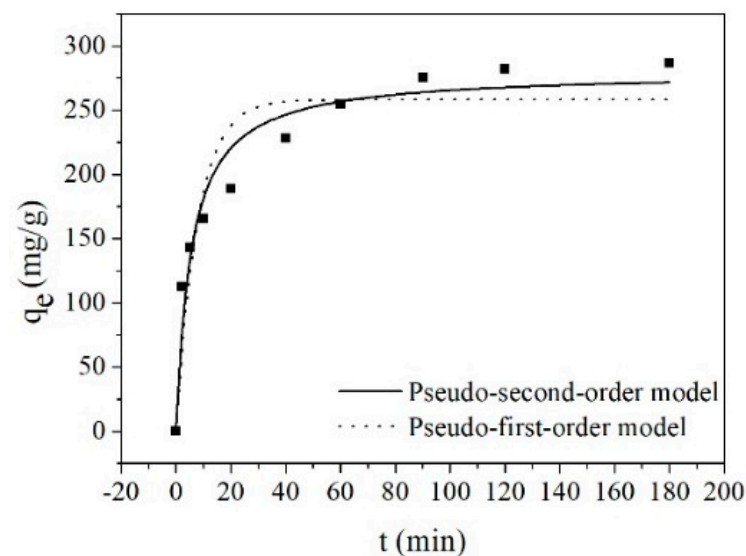
Figure 8. Adsorption kinetics of Pb(II) by LATP. (c_0 = 800 mg/L, T = 298 K, m = 2.0 g/L, V = 50 mL, pH = 4.5).

The Lagrange pseudo-first-order kinetic model and Lagrange pseudo-second -order kinetic model were selected for modeling the adsorption data to analyze the kinetic characteristics of adsorption [37].

The models can be written as follows:

Lagrange pseudo-first order kinetic model:

$$q_t = q_e\left(1-e^{-k_1 t}\right) \tag{3}$$

Lagrange pseudo-second order kinetic model:

$$q_t = \frac{q_e^2 k_2 t}{1 + q_e k_2 t} \tag{4}$$

where q_e and q_t are the adsorption capacities at adsorption equilibrium and at time of t respectively (mg/g), t is the adsorption time (min), k_1 is the first-order adsorption rate constant (min^{-1}), k_2 is the second-order adsorption rate constant, (g/mg min).

The kinetic parameters of Pb(II) adsorption on LATP (obtained from the nonlinear method) are summarized in Table 3. According to the high determination coefficient ($R^2 = 0.9462$), the pseudo-second-order kinetic model can well describe the experimental data of adsorption kinetics. It indicated that the adsorption was a chemical adsorption process [38].

Table 3. Kinetic parameters of Pb(II) adsorption on LATP.

Pseudo First-Order Model			Pseudo Second-Order Model		
q_e (mg/g)	k_1 (min^{-1})	R^2	q_e (mg/g)	k_2 (g/mg min)	R^2
258.22	0.1278	0.8690	279.76	6.6392×10^{-4}	0.9462

3.2.5. Adsorption Isotherms of Pb(II)

The effects of different initial Pb^{2+} concentrations on adsorption were tested at different temperatures. The experimental data were fitted by Langmuir isotherm and Freundlich isotherm models [39].

The models can be written as follows:

Langmuir isotherm equation:

$$q_e = \frac{b c_e q_m}{1 + b c_e} \tag{5}$$

Freundlich isotherm equation:

$$q_e = k c_e^{1/n} \tag{6}$$

where q_e is the adsorbing capacity at adsorption equilibrium (mg/g), c_e is the concentration of Pb^{2+} in the solution at adsorption equilibrium (mg/L), q_m is the saturation adsorption capacity of the adsorbent (mg/g), b is the Langmuir adsorption constant, k is a constant related to the adsorption capacity and n is an empirical parameter related to the adsorption intensity.

Adsorption isotherms of Pb(II) on LATP are shown in Figure 9, and the simulated adsorption parameters obtained from the isotherms are shown in Table 4. The results show that the Langmuir equation fitted the adsorption isotherm data of Pb(II) onto LATP well, and the Langmuir model was more suitable to describe the adsorption behavior of Pb(II) on LATP. It was supported by the higher correlation coefficients ($R_{298k}^2 = 0.9359$, $R_{308k}^2 = 0.9405$ and $R_{318k}^2 = 0.9840$) at different temperatures derived from the Langmuir model. It suggests that the adsorption of Pb(II) on LATP is a monolayer adsorption process [40]. The Langmuir model assumes that adsorption mainly takes place on a homogeneous surface [41], which indicates that the lignin homogeneous distributed on the surface of attapulgite and the microporous structures were filled. The fitting results also show that LATP has a high adsorption capacity, which increases with temperature.
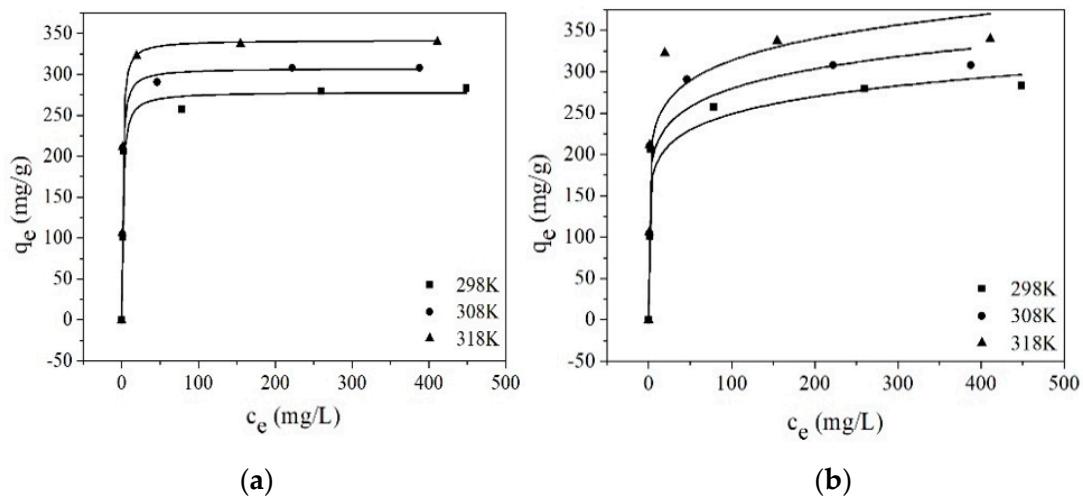
Figure 9. Langmuir (**a**) and Freundlich (**b**) isotherms of Pb(II) on LATP. (m(LATP) = 2.0 g/L, V = 50 mL, pH = 4.5).

Table 4. Isotherm parameters of Pb(II) adsorption on LATP.

Temperature (K)	Langmuir Equation			Freundlich Equation		
	q_m (mg/g)	b (L/mg)	R^2	k ((mg$^{1-(1/n)}$·L$^{1/n}$)/g)	$1/n$	R^2
298	286.40	0.1493	0.9359	116.88	0.1546	0.8882
308	315.51	0.2200	0.9405	138.15	0.1464	0.8715
318	349.70	0.3758	0.9840	168.32	0.1314	0.8484

3.2.6. Adsorption Thermodynamics

The adsorption thermodynamic parameters such as a change in Gibbs free energy (ΔG^0), enthalpy (ΔH^0) and entropy (ΔS^0) can predict the physical and chemical mechanisms of Pb(II) adsorption [42]. The parameters can be essentially estimated by the Van't Hoff equations [43].

The equations can be written as follows:

$$\ln K_C = \frac{-\Delta H^0}{RT} + \frac{\Delta S^0}{R} \tag{7}$$

$$\Delta G^0 = -RT \ln K_C \tag{8}$$

where K_C is the equilibrium constant (dimensionless); R is the universal gas constant (8.314; J/mol·K); and T is the absolute temperature in degrees Kelvin (K).

It was reported that the equilibrium constant K_C can be derived from the Langmuir constant, and the Langmuir constant was converted into K_C by the method reported by Tran [44]. ΔH^0 and ΔS^0 were obtained from the slope and intercept at the line plotted by $\ln K_C$ versus $1/T$, respectively. The values of ΔG^0 were calculated directly from Equation (6). The thermodynamics parameters of Pb(II) adsorption on LATP were presented in Table 5.

**Table 5.** Thermodynamics parameters of Pb(II) adsorption on LATP.

T (K)	ΔH^0 (kJ·mol^{-1})	ΔS^0 (J·mol^{-1}·K^{-1})	ΔG^0 (kJ·mol^{-1})
298 K			−29.52
308 K	36.29	220.59	−31.50
318 K			−33.94

The ΔG^0 values for the adsorption of Pb(II) were equal to −29.52, −31.50, −33.94 kJ·mol^{-1}, respectively. The negative ΔG^0 values indicated that the process of Pb(II) adsorption on

LATP occurred spontaneously. The ΔH^0 value was positive which indicated that the adsorption process was endothermic in nature. It provided theoretical foundation for the conclusion of adsorption capacity increased with the temperature. The positive ΔS^0 indicated that the adsorption process is entropy-driven rather than enthalpy-driven [45].

3.2.7. Reusability of LATP

The adsorption capacities of Pb(II) on LATP decreased with the decrease in pH. This suggests that the adsorption sites on LATP may be occupied by H^+ or that the absorbed Pb^{2+} on LATP may be desorbed by acid. In this study, 0.1 mol/L HNO_3 solution was used to desorb Pb^{2+} on LATP, and it was regenerated by using 0.1 mol/L $NaHCO_3$ solution in each set cycle experiment. The results of the cycling experiments are shown in Figure 10. There was a slight decrease in the adsorption capacity of the LATP, but the LATP still maintained 85% of the adsorption capacity of the fresh LATP after five cycles.
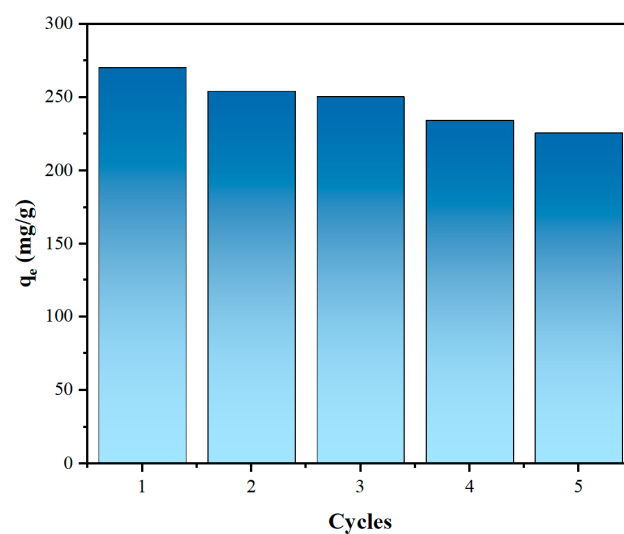

Figure 10. Reusability of LATP in Pb(II) adsorption.

3.3. Effect of Humic Acid on the Adsorption Capacity of LATP

Considering the prevalence of humic acid (HA) in polluted waters, the effect of HA on LATP treatment of mono and poly systems was investigated. As shown in Figure 11a, increasing the concentration of hydroxyapatite (HA) from 10 to 50 mg/L had a minimal impact on the maximum adsorption capacity and removal rate of Pb(II) by LATP. In the presence of a multivariate system, the addition of humic acid (HA) resulted in a decrease in the adsorption capacity of Pb(II) from 250.6 mg/g to 211.56 mg/g due to the competitive adsorption between Pb and HA. However, it did not affect the primary mechanism of Pb(II) removal by LATP. On the other hand, the addition of HA had the opposite effect on the removal of Cu and Cd. The enhancement of Cu removal could be attributed to the complexation between Cu and HA, forming Cu-HA complexes. At pH = 7, HA may weakly interact with the negative charges on the surface of LATP, occupying some of the active sites and leading to reduced Cd removal.

Overall, the experimental findings demonstrate that varying the concentration of HA does not significantly affect the maximum adsorption capacity and removal rate of Pb(II) by LATP. However, it does affect the removal of Cu and Cd, with an enhancement observed for Cu removal due to complexation with HA and a reduction in Cd removal due to the competitive occupation of active sites by HA.
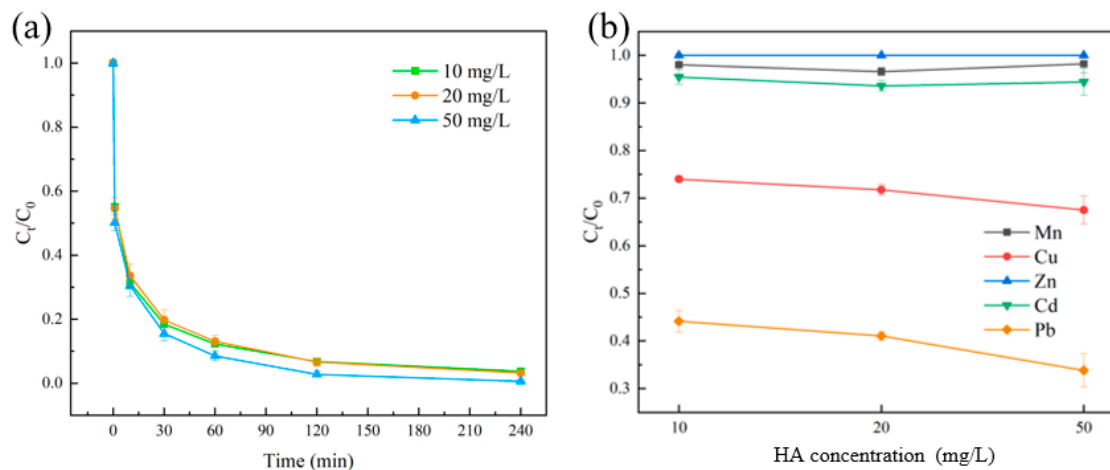
Figure 11. The effect of coexisting HA on LATP treatment of (**a**) Pb(II) and (**b**) multiple heavy metal ions. (C_0 = 600 mg/L, T = 298 K, m = 2.0 g/L, V = 50 mL, pH = 4.5).

3.4. Removing Mechanism

SEM and thermogravimetric analysis showed that the crystal structure and morphology of attapulgite are preserved and the carbonates are eliminated when the attapulgite is treated with low concentrations of acid [46]. It promoted the specific surface area of attapulgite and made the attapulgite have a larger adsorption capacity. The results of SEM and FTIR indicated that lignin was immobilized on ATP. The isotherm parameters and SEM graphs show that the lignin is homogeneous and distributed on the surface of attapulgite and the microporous structures were filled. The zeta potential test showed that LATP was negatively charged over the selected pH range. Therefore, LATP obtained the ability to adsorb metal cations by electrostatic attraction.

The adsorption proceeds of lignin to heavy metal ions were through ion- exchange mechanism [47]. The carboxyl groups and hydroxyl groups lignin account for the metallic ion adsorption performance of lignin, and the amount of hydroxyl groups is much greater than that of carboxyl groups, but their affinity towards different metal ions differs [20]. Surface complexation modeling analysis revealed that the phenolic groups bind the metallic ions before the carboxylic groups [48]. The binding strength for phenolic groups decreases in order Pb(II) > Cu(II) > Cd(II) > Zn(II) > Ni(II) and for carboxylic acid functional groups decreases in order Pb(II) > Cu(II) > Zn(II) > Cd(II) > Ni(II) [16]. The order of binding strength for phenolic groups is the same as the result of this study.

In conclusion, the adsorption mechanisms of heavy metals on the LATP surface may include electrostatic, ionic and complex adsorption. The dominant removal of Pb(II) may be attributed to its unique metal properties (lower hydration radius and negative logarithm of hydrolysis constant) and the fact that Pb(II) was a hard Lewis acid with a higher electronegativity (2.33). These properties may lead to Pb(II) possessing a greater affinity for the functional groups on LATP [28,29].

4. Conclusions

In this study, water-soluble lignin from black liquor was adsorbed and immobilized by activated attapulgite to make a new adsorbent (LATP). The results of SEM and FTIR show that lignin was successfully immobilized on attapulgite, and the attapulgite obtained a lot of function groups through the adsorption and immobilization of lignin, while a larger specific surface area and abundant pores were obtained during the acidification process. The possible modes of lignin connected to ATP may include physical adsorption, covalent bonding, non-covalent interactions, and ion exchange.

LATP showed advantageous adsorption of Pb(II) during the treatment of water polluted with a mixture of five heavy metal ions (Cd^{2+}, Pb^{2+}, Zn^{2+}, Mn^{2+}, Cu^{2+}), which was characterized by a greater removal mass and binding strength of Pb(II) than the other

ions. Because of surface protonation and deprotonation, the adsorption of Pb(II) by LATP was gradually enhanced with increasing pH. The adsorption of Pb(II) by LATP was in accordance with the pseudo-second-order kinetic model and the Langmuir model. The saturated adsorption capacity of LATP on Pb(II) reached 286.40 mg/g, 315.51 mg/g, and 349.70 mg/g at 298 K, 308 K, and 318 K, respectively. The adsorption of Pb(II) on LATP was spontaneous, and the adsorption process was endothermic in nature. LATP is reusable, and in the fifth cycle, the adsorption capacity of LATP for Pb(II) remained at about 85%. The mechanism of adsorption should be electrostatic attraction and ion exchange.

Cheap raw materials, a simple preparation process and excellent adsorption properties make the new adsorbent have a high application potential for removing heavy metal ions from wastewater.

Author Contributions: Conceptualization, X.L.; Methodology, S.G.; Software, S.G., J.G. and X.L.; Validation, S.G.; Formal analysis, Y.L., H.C. and J.G.; Investigation, Y.L., S.T. and H.C.; Resources, S.G., Y.L., H.C. and X.L.; Data curation, S.G. and S.T.; Writing—original draft, S.G., W.Z. and X.L.; Writing—review & editing, S.G., W.Z., Y.L., S.T. and X.L.; Visualization, W.Z.; Supervision, S.G., W.Z. and Y.L.; Project administration, X.L.; Funding acquisition, X.L. All authors have read and agreed to the published version of the manuscript.

Data Availability Statement: Data are contained within the article.

References

1. Duffus, J.H. "Heavy Metals"—A Meaningless Term. *Chem. Int.* **2002**, *23*, 163–167.
2. Bolan, N.S.; Choppala, G.; Kunhikrishnan, A.; Park, J.; Naidu, R. Microbial transformation of trace elements in soils in relation to bioavailability and remediation. *Rev. Environ. Contam. Toxicol.* **2013**, *225*, 1–56. [CrossRef]
3. Hamid, Y.; Tang, L.; Sohail, M.I.; Cao, X.; Hussain, B.; Aziz, M.Z.; Usman, M.; He, Z.L.; Yang, X. An explanation of soil amendments to reduce cadmium phytoavailability and transfer to food chain. *Sci. Total Environ.* **2019**, *660*, 80–96. [CrossRef]
4. Fu, F.; Wang, Q. Removal of heavy metal ions from wastewaters: A review. *J. Environ. Manag.* **2011**, *92*, 407–418. [CrossRef]
5. Ayansina, A.; Olubukola, B. A New Strategy for Heavy Metal Polluted Environments: A Review of Microbial Biosorbents. *Int. J. Environ. Res. Public Health* **2017**, *14*, 94. [CrossRef] [PubMed]
6. Fu, Y.; Liu, X.; Chen, G. Adsorption of heavy metal sewage on nano-materials such as titanate/TiO_2 added lignin. *Results Phys.* **2019**, *12*, 405–411. [CrossRef]
7. Jiang, C.; Wang, X.; Wang, G.; Hao, C.; Li, X.; Li, T. Adsorption performance of a polysaccharide composite hydrogel based on crosslinked glucan/chitosan for heavy metal ions. *Compos. Part B Eng.* **2019**, *169*, 45–54. [CrossRef]
8. Wang, S.; Sun, H.; Ang, H.M.; Tade, M.O. Adsorptive remediation of environmental pollutants using novel graphene-based nanomaterials. *Chem. Eng. J.* **2013**, *226*, 336–347. [CrossRef]
9. Ding, Z.; Hu, X.; Wan, Y.; Wang, S.; Gao, B. Removal of lead, copper, cadmium, zinc, and nickel from aqueous solutions by alkali-modified biochar: Batch and column tests. *J. Ind. Eng. Chem.* **2016**, *33*, 239–245. [CrossRef]
10. Efome, J.E.; Rana, D.; Matsuura, T.; Lan, C.Q. Insight Studies on Metal-Organic Framework Nanofibrous Membrane Adsorption and Activation for Heavy Metal Ions Removal from Aqueous Solution. *ACS Appl. Mater. Interfaces* **2018**, *10*, 18619–18629. [CrossRef]
11. Qin, W.; Qian, G.; Tao, H.; Wang, J.; Sun, J.; Cui, X.; Zhang, Y.; Zhang, X. Adsorption of Hg(II) ions by PAMAM dendrimers modified attapulgite composites. *React. Funct. Polym.* **2019**, *136*, 75–85. [CrossRef]
12. Liang, X.X.; Ouyang, X.K.; Wang, S.; Yang, L.Y.; Huang, F.; Ji, C.; Chen, X. Efficient adsorption of Pb(II) from aqueous solutions using aminopropyltriethoxysilane-modified magnetic attapulgite@chitosan (APTS-Fe_3O_4/APT@CS) composite hydrogel beads. *Int. J. Biol. Macromol.* **2019**, *137*, 741–750. [CrossRef] [PubMed]
13. Teng, Y.; Liu, Z.; Yao, K.; Song, W.; Sun, Y.; Wang, H.; Xu, Y. Preparation of Attapulgite/$CoFe_2O_4$ Magnetic Composites for Efficient Adsorption of Tannic Acid from Aqueous Solution. *Int. J. Environ. Res Public Health* **2019**, *16*, 2187. [CrossRef] [PubMed]
14. Deng, Y.; Gao, Z.; Liu, B.; Hu, X.; Wei, Z.; Sun, C. Selective removal of lead from aqueous solutions by ethylenediamine-modified attapulgite. *Chem. Eng. J.* **2013**, *223*, 91–98. [CrossRef]
15. Zhu, Y.; Fan, W.; Zhou, T.; Li, X. Removal of chelated heavy metals from aqueous solution: A review of current methods and mechanisms. *Sci. Total Environ.* **2019**, *678*, 253–266. [CrossRef]
16. Supanchaiyamat, N.; Jetsrisuparb, K.; Knijnenburg, J.T.N.; Tsang, D.C.W.; Hunt, A.J. Lignin materials for adsorption: Current trend, perspectives and opportunities. *Bioresour. Technol.* **2019**, *272*, 570–581. [CrossRef] [PubMed]

17. Li, C.; Zhao, X.; Wang, A.; Huber, G.W.; Zhang, T. Catalytic Transformation of Lignin for the Production of Chemicals and Fuels. *Chem. Rev.* **2015**, *115*, 11559–11624. [CrossRef]

18. Jin, Y.; Zeng, C.; Lü, Q.-F.; Yu, Y. Efficient adsorption of methylene blue and lead ions in aqueous solutions by 5-sulfosalicylic acid modified lignin. *Int. J. Biol. Macromol.* **2019**, *123*, 50–58. [CrossRef] [PubMed]

19. Yan, M.; Li, Z. Microwave-assisted functionalized lignin with dithiocarbamate for enhancing adsorption of Pb(II). *Mater. Lett.* **2016**, *170*, 135–138. [CrossRef]

20. Guo, X.; Zhang, S.; Shan, X.Q. Adsorption of metal ions on lignin. *J. Hazard. Mater.* **2008**, *151*, 134–142. [CrossRef]

21. Brdar, M.; Šćiban, M.; Takači, A.; Došenović, T. Comparison of two and three parameters adsorption isotherm for Cr(VI) onto Kraft lignin. *Chem. Eng. J.* **2012**, *183*, 108–111. [CrossRef]

22. Gao, S.; Zhao, J.; Wang, X.; Guo, Y.; Han, Y.; Zhou, J. Lignin Structure and Solvent Effects on the Selective Removal of Condensed Units and Enrichment of S-Type Lignin. *Polymers* **2018**, *10*, 967. [CrossRef] [PubMed]

23. Zhou, H.; Li, J.; Ma, E. Multiscale Modification of Populus cathayana by Alkali Lignin Combined with Heat Treatment. *Polymers* **2018**, *10*, 1240. [CrossRef] [PubMed]

24. Reyes-Rivera, J.; Soto-Hernández, M.; Canché-Escamilla, G.; Terrazas, T. Structural Characterization of Lignin in Four Cacti Wood: Implications of Lignification in the Growth form and Succulence. *Front. Plant Sci.* **2018**, *9*, 1518. [CrossRef]

25. Wang, S.; Yu, Y.; Di, M. Green Modification of Corn Stalk Lignin and Preparation of Environmentally Friendly Lignin-Based Wood Adhesive. *Polymers* **2018**, *10*, 631. [CrossRef]

26. Peng, L.; Zhou, L.; Li, Y.; Pan, F.; Zhang, S. Synthesis and properties of waterborne polyurethane/attapulgite nanocomposites. *Compos. Sci. Technol.* **2011**, *71*, 1280–1285. [CrossRef]

27. Tolia, G.; Li, S.K. Silicone Adhesive Matrix of Verapamil Hydrochloride to Provide pH-Independent Sustained Release. *AAPS PharmSciTech* **2014**, *15*, 1–10. [CrossRef]

28. Ni, B.-J.; Huang, Q.-S.; Wang, C.; Ni, T.-Y.; Sun, J.; Wei, W. Competitive adsorption of heavy metals in aqueous solution onto biochar derived from anaerobically digested sludge. *Chemosphere* **2019**, *219*, 351–357. [CrossRef] [PubMed]

29. Ren, J.; Zheng, L.; Su, Y.; Meng, P.; Zhou, Q.; Zeng, H.; Zhang, T.; Yu, H. Competitive adsorption of Cd(II), Pb(II) and Cu(II) ions from acid mine drainage with zero-valent iron/phosphoric titanium dioxide: XPS qualitative analyses and DFT quantitative calculations. *Chem. Eng. J.* **2022**, *445*, 136778. [CrossRef]

30. Zhang, L.; Zeng, Y.; Cheng, Z. Removal of heavy metal ions using chitosan and modified chitosan: A review. *J. Mol. Liq.* **2016**, *214*, 175–191. [CrossRef]

31. Fan, Q.; Li, Z.; Zhao, H.; Jia, Z.; Xu, J.; Wu, W. Adsorption of Pb(II) on palygorskite from aqueous solution: Effects of pH, ionic strength and temperature. *Appl. Clay Sci.* **2009**, *45*, 111–116. [CrossRef]

32. Huang, X.; Wei, D.; Zhang, X.; Fan, D.; Sun, X.; Du, B.; Wei, Q. Synthesis of amino-functionalized magnetic aerobic granular sludge-biochar for Pb(II) removal: Adsorption performance and mechanism studies. *Sci. Total Environ.* **2019**, *685*, 681–689. [CrossRef] [PubMed]

33. Zhou, L.C.; Li, Y.F.; Bai, X.; Zhao, G.H. Use of microorganisms immobilized on composite polyurethane foam to remove Cu(II) from aqueous solution. *J. Hazard. Mater.* **2009**, *167*, 1106–1113. [CrossRef] [PubMed]

34. Kapoor, A.; Viraraghavan, T.; Cullimore, D.R. Removal of heavy metals using the fungus Aspergillus niger. *Bioresour. Technol.* **1999**, *70*, 95–104. [CrossRef]

35. Han, L.; Jiang, B.; Wang, W.; Wang, G.; Tan, Y.; Niu, K.; Fang, X. Alleviating Nonproductive Adsorption of Lignin on CBM through the Addition of Cationic Additives for Lignocellulosic Hydrolysis. *ACS Appl. Bio Mater.* **2022**, *5*, 2253–2261. [CrossRef]

36. Lvov, Y.; Wang, W.; Zhang, L.; Fakhrullin, R. Halloysite Clay Nanotubes for Loading and Sustained Release of Functional Compounds. *Adv. Mater.* **2016**, *28*, 1227–1250. [CrossRef] [PubMed]

37. Ho, Y.S.; Mckay, G. Pseudo-second order model for sorption processes. *Process Biochem.* **1999**, *34*, 451–465. [CrossRef]

38. Wang, A.; Si, Y.; Yin, H.; Chen, J.; Huo, J. Synthesis of Na-, Fe-, and Mg-containing titanate nanocomposites starting from ilmenite and NaOH and adsorption kinetics, isotherms, and thermodynamics of Cu(II), Cd(II), and Pb(II) cations. *Mater. Sci. Eng. B* **2019**, *249*, 114411. [CrossRef]

39. Zhang, B.; Shi, W.; Yu, S.; Zhu, Y.; Zhang, R.; Tay, J.H. Adsorption of anion polyacrylamide from aqueous solution by polyte-trafluoroethylene (PTFE) membrane as an adsorbent: Kinetic and isotherm studies. *J Colloid Interface Sci* **2019**, *544*, 303–311. [CrossRef]

40. Zhang, C.; Xiao, Y.; Qin, Y.; Sun, Q.; Zhang, S. A novel highly efficient adsorbent {[Co$_4$(L)$_2$(μ_3-OH)2(H$_2$O)$_3$(4,4′-bipy)$_2$]·(H$_2$O)$_2$}n: Synthesis, crystal structure, magnetic and arsenic (V) absorption capacity. *J. Solid State Chem.* **2018**, *261*, 22–30. [CrossRef]

41. Sun, J.; Zhang, X.; Zhang, A.; Liao, C. Preparation of Fe–Co based MOF-74 and its effective adsorption of arsenic from aqueous solution. *J. Environ. Sci.* **2019**, *80*, 197–207. [CrossRef] [PubMed]

42. Tran, H.N.; You, S.-J.; Chao, H.-P. Thermodynamic parameters of cadmium adsorption onto orange peel calculated from various methods: A comparison study. *J. Environ. Chem. Eng.* **2016**, *4*, 2671–2682. [CrossRef]

43. Tomul, F.; Arslan, Y.; Basoglu, F.T.; Babuccuoglu, Y.; Tran, H.N. Efficient removal of anti-inflammatory from solution by Fe-containing activated carbon: Adsorption kinetics, isotherms, and thermodynamics. *J. Environ. Manag.* **2019**, *238*, 296–306. [CrossRef] [PubMed]

44. Tran, H.N.; You, S.J.; Hosseini-Bandegharaei, A.; Chao, H.P. Mistakes and inconsistencies regarding adsorption of contaminants from aqueous solutions: A critical review. *Water Res.* **2017**, *120*, 88–116. [CrossRef] [PubMed]

45. Yang, J.; Yu, M.; Qiu, T. Adsorption thermodynamics and kinetics of Cr(VI) on KIP210 resin. *J. Ind. Eng. Chem.* **2014**, *20*, 480–486. [CrossRef]
46. Boudriche, L.; Calvet, R.; Hamdi, B.; Balard, H. Effect of acid treatment on surface properties evolution of attapulgite clay: An application of inverse gas chromatography. *Colloids Surf. A Physicochem. Eng. Asp.* **2011**, *392*, 45–54. [CrossRef]
47. Albadarin, A.B.; Al-Muhtaseb, A.a.H.; Al-laqtah, N.A.; Walker, G.M.; Allen, S.J.; Ahmad, M.N.M. Biosorption of toxic chromium from aqueous phase by lignin: Mechanism, effect of other metal ions and salts. *Chem. Eng. J.* **2011**, *169*, 20–30. [CrossRef]
48. Ge, Y.; Li, Z. Application of Lignin and Its Derivatives in Adsorption of Heavy Metal Ions in Water: A Review. *ACS Sustain. Chem. Eng.* **2018**, *6*, 7181–7192. [CrossRef]